Research papers

Role of wind in regulating phytoplankton blooms on the Mid-Atlantic Bight

Y. Xu *, B. Cahill, J. Wilkin, O. Schofield

Coastal Ocean Observation Lab, Institute of Marine and Coastal Sciences, School of Environmental and Biological Sciences, Rutgers University, New Brunswick, NJ, 08901, US

ARTICLE INFO

ABSTRACT

Mixing has long been recognized as having an important role in influencing underwater light and nutrient budgets and thus regulating phytoplankton bloom. Mixing related to stratification and de-stratification is a key parameter of the physical environment that can control the timing and magnitude of blooms. Here we use a high-resolution three-dimensional biogeochemical model in the Mid-Atlantic Bight (MAB) to study phytoplankton bloom dynamics for the years 2004–2007. We present a simulated fall-winter bloom in the shelf region and spring bloom in the shelf-break front region. The ratio of light over mixed layer depth (MLD) was used to determine the trade-off effects of mixing (increase mixing will increase nutrients availability but decrease light availability). We find that the critical light value ($I'_{chl\ mas}$) is around 60 (W m^{-2}) for the shelf region and 150 (W m^{-2}) for the shelf-break front region. There is a predictable linear regression relationship between $I'_{chl\ mas}$ and depth. A sensitivity run with no wind forcing was used to test the role of wind-induced mixing on the balance between light and nutrient terms and its influence on timing and magnitude of the bloom. The phytoplankton dynamics in the shelf-break front region are found to be more sensitive to the wind-induced mixing.

Published by Elsevier Ltd.

1. Introduction

Broad continental shelves are highly productive systems that are globally significant zones for the biogeochemical cycling of elements (Longhurst, 1998). This is especially true for the Mid-Atlantic Bight (MAB), which has an extremely productive ecosystem that is fueled by large seasonal phytoplankton blooms (O'Reilly and Busch, 1984; O'Reilly et al., 1987). This has motivated numerous observational studies on the physical forcing of phytoplankton blooms in the MAB. These studies have documented the spatial and temporal variability in phytoplankton biomass in the MAB and have hypothesized about the key physical processes that underlie the observed variability. The 12 yr (1977–1988) NOAA NMFS Marine Resource Monitoring and Prediction (MARMAP) survey of the Northeast of US continental shelf found the highest phytoplankton concentrations during the winter-spring (O'Reilly and Zetlin, 1998). This was consistent with previous results from the Coastal Zone Color Scanner (CZCS) and Sea-viewing Wide Field of view Sensor (SeaWiFS) imagery that showed a fall-winter maximum of chlorophyll concentration in the middle and outer shelf waters and a spring maximum in the shelf-break/slope waters (Ryan et al., 1999; Xu et al., 2011; Yoder et al., 2001). Despite these large data sets, the observational studies did not have the spatial and temporal data required to

link the environmental factors that underlie the phytoplankton dynamics. This has prompted the development of coupled eco-system models to test hypotheses about the physical regulation of the MAB phytoplankton communities (Fennel et al., 2006).

Models describing phytoplankton dynamics must reconcile a phytoplankton's need for light and nutrients, both of which are related to the overall mixing in the water column. The limitation of light to support phytoplankton growth builds on the (Sverdrup, 1953) "critical depth" model which predicts the initiation of phytoplankton blooms only after cells reside at a the critical depth where photosynthesis is larger than respiration allowing for the build-up of biomass. The maximum depth suitable for phytoplankton photosynthesis is most often defined as the depth where photosynthetic available radiation (PAR) is 1% of its surface value. While the absolute lower limit of light capable of supporting photosynthesis is still a subject of debate (Dubinsky and Schofield, 2010), estimates of the compensation depth irradiance based on Sverdrup's theory suggest it is relatively uniform throughout many regions of the ocean (Siegel et al., 2002). If light is present in sufficient quantities, the magnitude and duration of the bloom is then a complex function of mixing, nutrient availability (Tilman, 1982) and grazing pressure (Fasham et al., 1990; Gentleman et al., 2003; Martin, 1965; Turner and Tester, 1997). The flux of nutrients to the euphotic zone is determined by mixing across the nutricline, which can happen with mixed layer depth (MLD) increase if it is associated with entrainment. MLD thus has been demonstrated to be a key factor in determining phytoplankton abundance (Behrenfeld et al.,

* Corresponding author.
  E-mail address: xumeihao@gmail.com (Y. Xu).

2002; Field et al., 1998); however while vertical mixing in the upper-ocean boundary layer can increase productivity in the surface waters through enhanced nutrient supply from deep waters it can also decrease productivity due to mixing phytoplankton below the critical depth and therefore introducing the possibility of light limitation (Dutkiewicz et al., 2001). To parameterize the relative roles of mixing and light availability the ratio of Z_{mld} (mixing layer depth) to Z_{eu} (euphotic depth) has been used to describe the regulating primary production (Huisman et al., 1999; Irigoien and Castel, 1997); however, this ratio only reflects the relationship between surface light condition and MLD. Therefore, the ratio of integral of light in the euphotic zone and MLD ($\int_{-Z_{eu}}^{0} I(z)dz/z_{mld}$) might be a preferred value to compare the balance between light limitation and nutrient limitation.

We use time series of satellite chlorophyll and 3-D biophysical model simulations to investigate the relative importance of mixing rates and light availability for phytoplankton populations in the MAB.

2. Methods

For this project we utilized data collected by the Mid-Atlantic Regional Coastal Ocean Observing System (MARCOOS) that is part of the United States Integrated Ocean Observing System (IOOS) (Schofield et al., 2010). MARCOOS provided an extensive data set to validate biological model simulations. In this effort we used surface data provided by ocean color satellite imagery and in situ data collected by Webb Slocum gliders (Schofield et al., 2007).

2.1. The biogeochemical model

In this study we used the Regional Ocean Modeling System (ROMS, http://www.myroms.org) (Haidvogel and Beckmann, 1999; Wilkin et al., 2005) which was configured to the continental shelf of the Middle Atlantic Bight (MAB) (the model domain is shown in Fig. 1). The model has a horizontal grid resolution of approximately 5 km, and uses 36 vertical layers in a terrain-following s-coordinate system. The biogeochemical model was developed and described in Fennel et al. (2006). The model here assumes nitrogen is the major limiting nutrient, which is a reasonable assumption as nutrient budgets indicate nitrogen limitation is frequently observed in the MAB (Ryther and Dunstan, 1971; Sharp and Church, 1981). Also nitrogen availability in the MAB is found the key nutrient to accurately simulating primary production (Fennel et al., 2006). The basic structure of this model follows a classical Fasham model (Fasham et al., 1990) and is constructed using seven state variables: phytoplankton, zooplankton, nitrate, ammonium, small and large detritus, and chlorophyll. The time rate change of phytoplankton is influenced by the growth rate of phytoplankton, grazing by zooplankton, mortality, aggregation of phytoplankton to small and large detritus, and vertical sinking of the aggregates. This model drives phytoplankton growth (μ) through variations in temperature (T) (Eppley, 1972), incident light intensity (I) (Evans and Parslow, 1985), and the availability of nutrients (Parker, 1993), following:

$$\mu = \mu_{max} f(I)(L_{NO_3} + L_{NH_4})$$ (1)

μ_{max} is the maximum growth rate which depends on temperature. I is the photosynthetically available radiation and decreases with water depth due to absorption by seawater (assumed constant) and the time and spatially varying chlorophyll computed by the model.

$$I = I(z) = I_0 par \ exp-z(K_w + K_{chl} \int_z^0 Chl(\zeta)d\zeta)$$ (2)
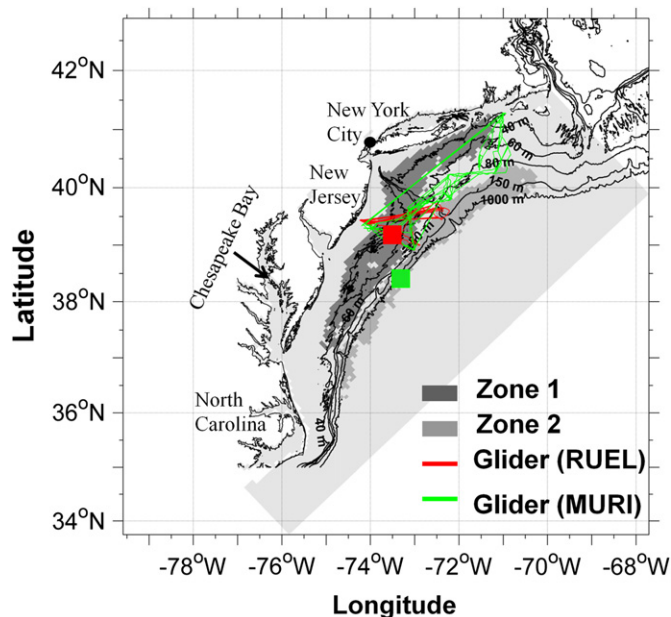
Fig. 1. Model domain (light gray). Dark gray and gray highlight the Zone 1 and Zone 2 region identified by Xu et al. (2011). Red and green lines show the glider transects. Red and green square symbols represent the grid point used for calculation in Zone 1 and Zone 2. The black lines with number show the bathymetry. (For interpretation of the references to color in this figure legend, the reader is referred to the web version of this article.)

where I_0 is the surface incoming light and is the shortwave radiation flux from NCEP reanalysis data, *par* is the fraction of light that is available for photosynthesis and equals 0.43. K_w and K_{chl} are the light attenuation coefficients for water and chlorophyll, and are set to 0.04 m^{-1} and 0.025 (mg Chl)$^{-1}$ m^{-2} respectively (Fennel et al., 2006). The $f(I)$ represents the photosynthesis-light (P–I) relationship. The parameter α is the initial slope of the P–I curve. The terms L_{NO_3} and L_{NH_4} represents the nutrients limitation.

$$f(I) = \frac{\alpha I}{\sqrt{\mu_{max}^2 + \alpha^2 I^2}},$$ (3)

$$L_{NO_3} = \frac{NO_3}{K_{NO_3} + NO_3} \frac{1}{1 + NH_4/K_{NH_4}},$$ (4)

$$L_{NH_4} = \frac{NH_4}{K_{NH_4} + NH_4}$$ (5)

The rate of grazing by zooplankton is represented by a Holling type s-shaped curve (Gentleman et al., 2003). The mortality loss term has linear relationship with phytoplankton. The aggregation rate is assumed to scale with the square of small particle abundance for more details see Fennel et al., 2006. The model was driven by atmospheric forcing provided by the North American R (NAM) forecast regional Reanalysis (NARR) from the National Centers for Environmental Prediction (NCEP). We used a 3-hourly re-analysis of surface air temperature, pressure, relative humidity, 10 m vector winds, precipitation, downward long-wave radiation, and net shortwave radiation to specify the surface fluxes of momentum and buoyancy using bulk formulae (Fairall et al., 2003). In the open boundary, we specified temperature, salinity, nitrate (NO$_3$), total inorganic carbon (TIC), alkalinity, and oxygen. Because the focus of this study is the influence of wind forcing on phytoplankton dynamics, the open boundary inputs are specified by the climatology input based on the Fennel ROMS model simulation of the Northeast North American (NENA) shelf (Fennel et al., 2006). We included the inputs of seven rivers

(Hudson, Connecticut, Delaware, Susquehanna, Potomac, Choptank, and James River) on the boundary. River outflow was provided by the daily mean outflow from the United States Geological Survey (USGS) gauges (available online at http://water data.usgs.gov/nwis/). The riverine inputs of temperature, salinity, dissolved and particulate biological constituent concentrations were derived from the total nitrogen in the nitrate pool after Howarth et al., (1996). Here the inputs were multiplied by the freshwater transport to give discharge rates, which for our simulations was treated as time invariant. The model is initialized with model output in this domain described in Hofmann et al. (2011). The 4 yr (2004–2008) duration simulations were conducted with the first year used as a spin-up period; results presented here are from the analysis of the final three-years of simulation.

2.2. Satellite imagery

Seasonal cycles in MAB phytoplankton were characterized using four-day averaged nine-year time series of surface chlorophyll concentration derived from Sea-viewing Wide Field of view Sensor (SeaWiFS) ocean color imagery from January 1998 to December 2006. Images with more than 20% cloud coverage were excluded. Therefore we utilized the 4-day composite, which was the minimum time interval that minimized cloud contamination and provided a reasonable time series that could define seasonal phytoplankton dynamics on the shelf. Even using the 4-day average 43% of imagery was eliminated from the data set. The missing data was largest in the fall-winter in each year. The monthly SeaWiFS Level 3 photosynthetically available radiation (PAR) data from 1998 to 2006 were downloaded from http://oceancolor.gsfc.nasa.gov. We used the spatial mean for both chlorophyll-a and PAR for the shelf and shelf-break front regions (Zone 1 and Zone 2, as showed in Fig. 1 dark gray and gray area respectively) identified in Xu et al. (2011). The two zones were defined by a decadal Empirical Orthogonal Function analysis of ocean color imagery, which identified two major modes of variability. The first mode (Zone 1) was associated with the inner

continental shelf of the MAB spanning the 20–60 m isobaths. Zone 1 was defined by the fall-winter bloom of phytoplankton (Xu et al., 2011). Zone 2 was located in the 80–150 m isobaths located at the edge of the MAB continental slope and was associated with the spring phytoplankton bloom.

2.3. Glider Observations

We utilized Webb Slocum gliders for this study (Schofield et al., 2007). The data was collected as part of local and regional glider time series in the MAB (Schofield et al., 2010, Fig. 1). The time series is not formally funded and thus is not a complete monthly time series; however the time series is a large data base providing vertical profiles of temperature and salinity. A smaller subset of chlorophyll data was available, however it should be noted that not every glider is equipped with a fluorometer. The data base used for this study spans from 2006 to 2008. During the periods, there are three missions (June 2006, July 2006, and July 2007) along Rutgers University Glider Endurance Line (RUEL) and three missions (March 2007, April 2007, and March 2008) along Multidisciplinary University Research Initiative Line (MURI). For the RUEL transect, it takes approximately 5–10 days to be completed, while for the MURI transect, it takes 12–25 days to be completed. The majority of the glider observations provide data for spring and summer time. These efforts provide over 8257 vertical profiles with temperature, salinity and chlorophyll data that were included in this study. All gliders are equipped with a Sea-Bird conductivity-temperature-depth (CTD) sensor. The MLDis based on the measurement of temperature and salinity and is defined using the criterion of a 0.125 kg m^{-3} density increase from the surface.

3. Results

3.1. Model simulation and observations of MAB phytoplankton

We have focused our analysis of the seasonal variability in phytoplankton in Zone 1 and Zone 2 as identified in Xu et al. (2011). Time series of the 4-day average spatial mean SeaWiFS
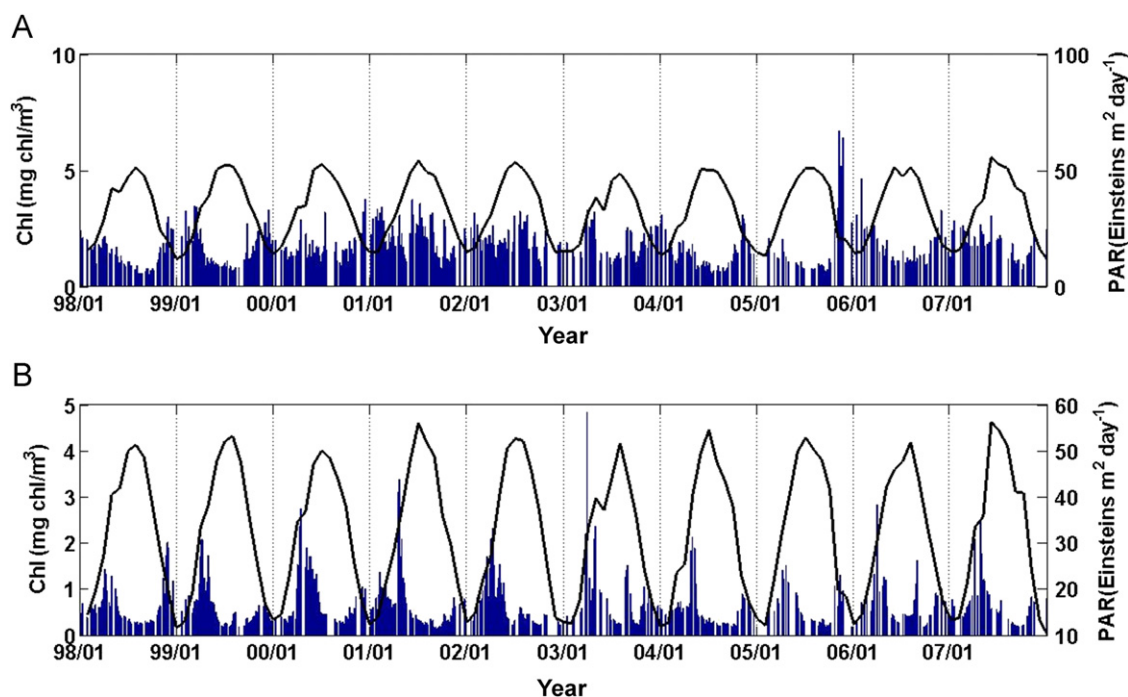

Fig. 2. The 9-year record of SeaWiFS chlorophyll (bar) compared to photosynthetically active radiation (PAR, black line) from the spatial mean in (A) Zone 1 and (B) Zone 2.

chlorophyll for both zones is shown in Fig. 2. Generally, the chlorophyll in Zone 1 showed a persistent phytoplankton bloom in the late fall and winter that typically lasted several weeks despite the solar illumination being lowest during this time of year. The timing of this bloom has been related to the seasonal destratification of the MAB, which replenishes nutrients to the surface waters. The magnitude of bloom has been related to the overall wind-induced mixing with the frequency of winter storms determining the overall seasonal light-limitation of the phytoplankton (Xu et al.,

2011). In contrast, the phytoplankton blooms in Zone 2 occur in the spring and are associated with the onset of stratification in the deeper waters of the outer shelf (Fig. 2B). The spring bloom is shorter and has lower concentrations of chlorophyll than the fall-winter bloom. These seasonal cycles of chlorophyll are consistent with the in situ MARMAP data (Yoder et al., 2001, shown in Fig. 6), that show peak chlorophyll values occur during fall-winter in middle and outer shelf water and a distinct spring maximum in shelf-break slope waters (Yoder et al., 2001).

The satellite measured chlorophyll dynamics were successfully reproduced by the biological model (Fig. 3). The simulated sea surface temperature was also in the standard deviation range when compare with the climatology measurement from NDBC buoy 44009 (Fig. 4C). The simulated chlorophyll in Zone 1 increased in late fall and lasted through the winter. The correlation found between simulated chlorophyll and SeaWiFS chlorophyll was 0.48 ($p < 0.001$, Fig. 4A) which was mainly due to the winter bloom. The bloom showed a bimodal peak with lower concentrations found during the darkest periods of winter which was not readily evident in the satellite data that perhaps reflect the relatively low availability of ocean color images during the cloudy winter (Xu et al., 2011). The model also successfully simulated the timing and magnitude of spring bloom in Zone 2, which could explain ∼74% of the log-transformed variance of the observed chlorophyll ($p < 0.001$, Fig. 4B).

The model overestimated observed chlorophyll and likely reflects the poor prediction of zooplankton grazing for the following reasons. During the SEEP II experiments in this area (Flagg et al., 1994), zooplankton concentrations ranged from 0.4–28.6 mmol N m^{-3}. Our modeled zooplankton concentrations varied from 0 to 2 mmol N m^{-3}, which is within the range observed during SEEP II (Flagg et al., 1994) but at the lower end the observations. If grazing pressures were too low, then major factor regulating the termination of the spring bloom in the model would be the depletion of nutrients. This would result in the modeled spring bloom lasting longer than the satellite observations if zooplankton is significant in driving bloom senescence. The spring bloom based on the 4-day average SeaWiFS data typically lasted 12–20 days over a 10-year data set (Fig. 2B). The spring bloom in the model simulations typically lasted for 30–40 days (Fig. 3B), which would be consistent with the model that underestimating grazing pressure.

Fig. 3. Time series of surface chlorophyll concentration (black line) and net heat flux (gray line) of spatial mean in Zone 1 and Zone 2 calculated from model output.

Fig. 4. Comparison between the log-transformed surface chlorophyll concentrations provide by SeaWiFS and mode output from spatial mean of Zone 1 and Zone 2. The linear correlation of the chlorophyll before log-transformed is 0.42 and 0.75 (P value < 0.001) for Zone 1 and Zone 2 respectively. The climatology of surface water temperature from the NDBC buoy 44009 (the red line with error bar) was used to compare with the simulated SST at the same location (blue line) in Fig. 4C. (For interpretation of the references to color in this figure legend, the reader is referred to the web version of this article.)

3.2. Environmental regulation of phytoplankton

Accepting that the model describes the general variability observed for chlorophyll (Fig. 4), we used the model simulations to analyze the physical factors regulating phytoplankton biomass on the MAB. Time series of the modeled chlorophyll and key environmental variables (temperature, upper mixed layer, light, nutrients, and zooplankton) for both zones are shown in Figs. 5 and 6. In Zone 1(Fig. 5), water column cooling resulted in destratification, which was reflected as an increase in the upper mixed layer depth from 10 m at the beginning of October to 30 m deep at the end of February. The deepening of the upper mixed layer depth was associated with an increase of nitrate within the euphotic zone. Nitrate exhibited considerable variability within the upper 20 m showing that convective overturn and entrainment processes were effective increasing nutrients in surface waters. Nitrate within the mixed layer was consumed rapidly by phytoplankton from December to March. Phytoplankton growth was significant even during the dim winter months as > 50% of the water column was above the 1% light level depth. Phytoplankton biomass remained high until the upper mixed layer depth began to shallow and nitrate was rapidly depleted and grazing pressure increased. After surface
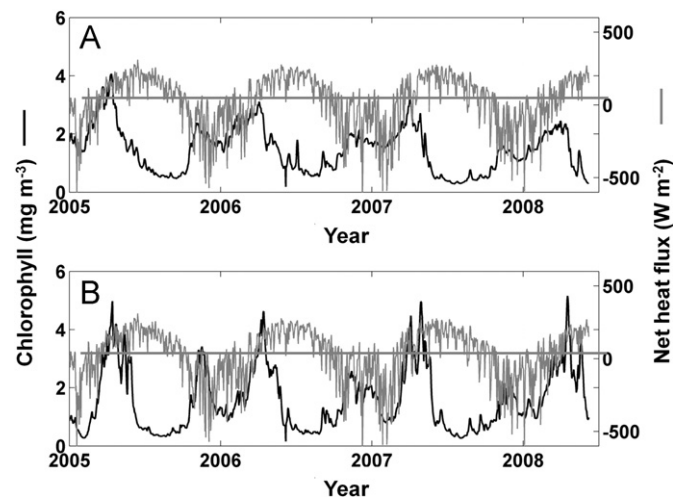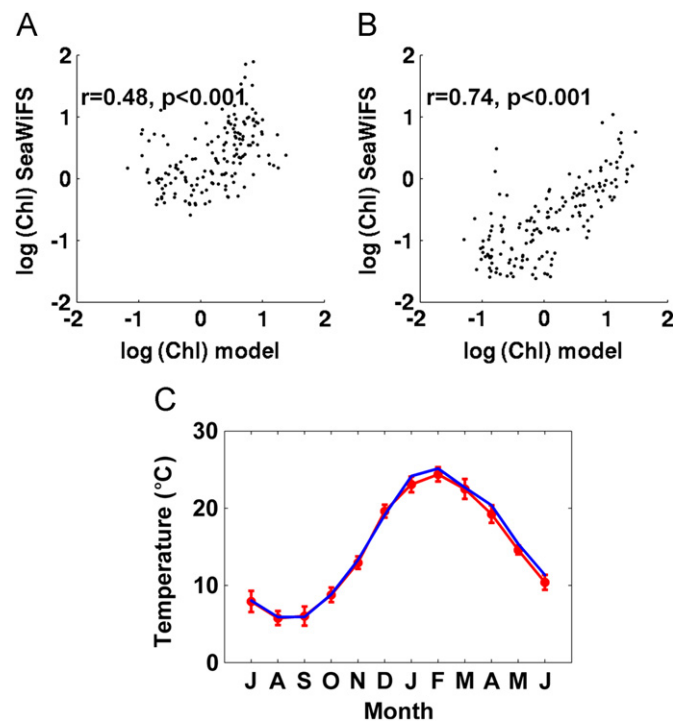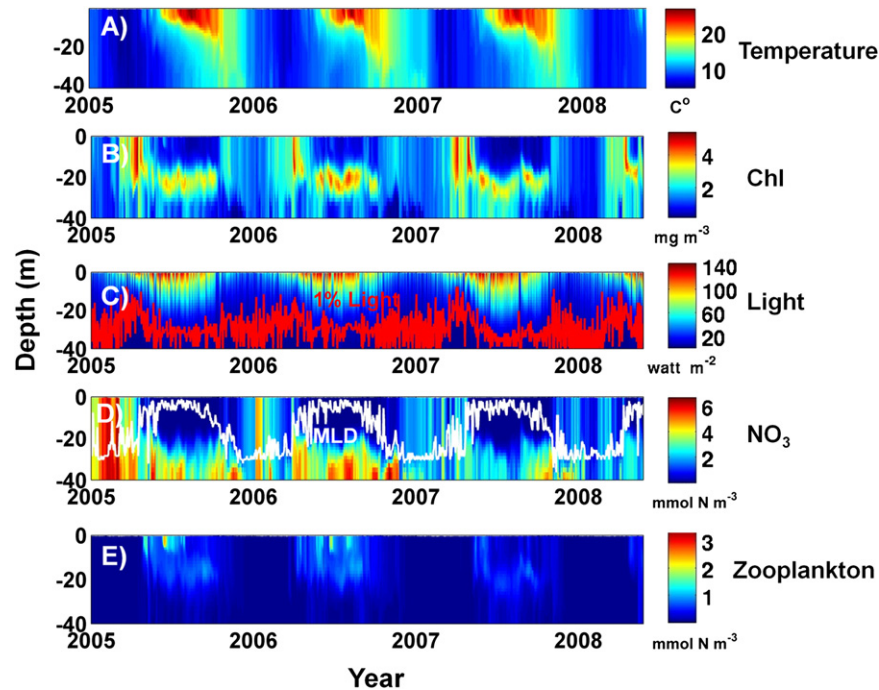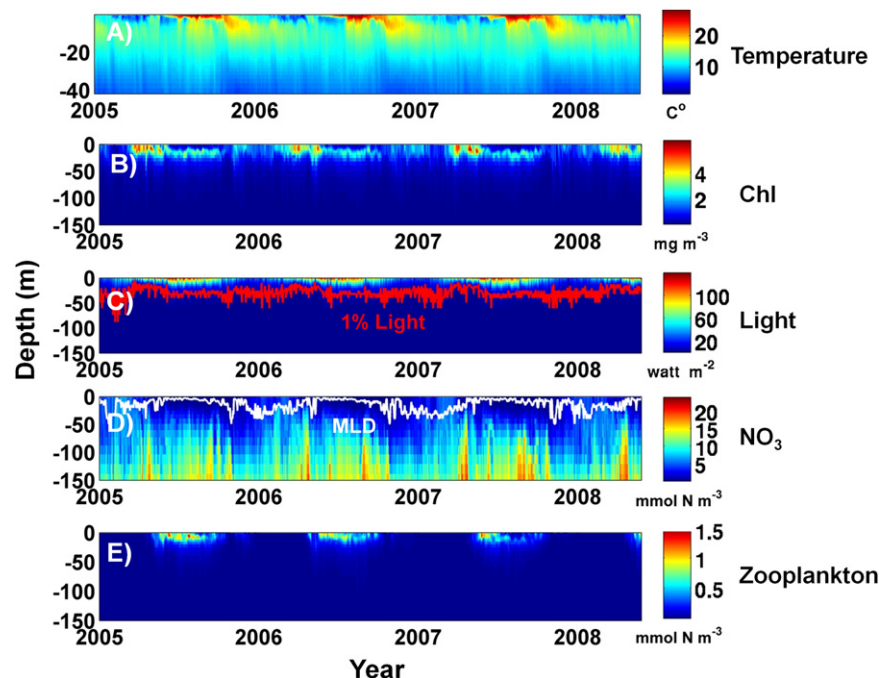
Fig. 5. Model simulated vertical distribution of temperature (A) chlorophyll concentration (B), light (C), NO₃ (D) and zooplankton (E) at a point located in Zone 1 (dot shown in Fig. 1). The 1% light level depth is plotted with light (in C, red line) and the MLD is plotted with NO₃ (in D, white line). (For interpretation of the references to color in this figure legend, the reader is referred to the web version of this article.)


Fig. 6. Model simulated vertical distribution of temperature (A) chlorophyll concentration (B), light (C), NO₃ (D) and zooplankton (E) at a point located in Zone 2 (square shown in Fig. 1). The 1% light level depth is plotted with light (in C red line) and the MLD is plotted with NO₃ (in D, white line). (Here, we only show the upper 150 m of the water column). (For interpretation of the references to color in this figure legend, the reader is referred to the web version of this article.)

nitrate was depleted, a significant subsurface phytoplankton peak was maintained at the nutricline throughout the year.

In contrast, phytoplankton blooms in Zone 2 were found primarily in the spring with a smaller secondary bloom in the fall when stratification began to weaken (Fig. 6). No winter phytoplankton bloom was observed as the upper mixed layer was deep and the majority of the water column was below the 1% light level (Xu et al., 2011). The spring phytoplankton bloom formed in March every year during the simulation as the upper mixed layer depth decreased and nitrate concentrations were high. The nutrients were consumed in several weeks and nutrient depletion resulted in the termination of the bloom. As observed in Zone 1, a subsurface phytoplankton bloom formed, however the nutricline was deep and the subsurface concentrations of chlorophyll were less than half then observed on the inner continental shelf.
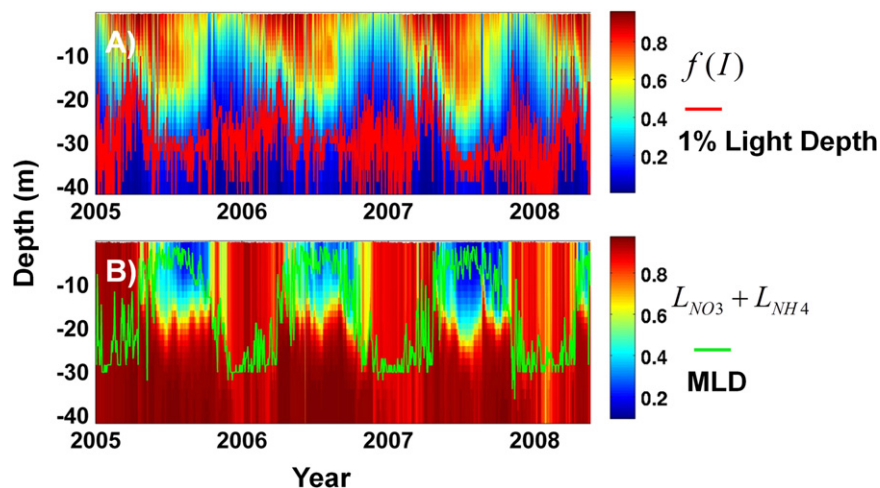
Fig. 7. Vertical distribution of limitation function of light (A) and nutrient (B) at a point located in Zone 1 (dot shown in Fig. 1). The 1% light level depth is plotted with function of light (in A, red line) and the MLD is plotted with nutrient limitation function (in (B), white line). (For interpretation of the references to color in this figure legend, the reader is referred to the web version of this article.)

The relative limitation of phytoplankton by light and nutrients is tightly coupled to the depth of the upper mixed layer as is illustrated in Fig. 7. The threshold for light limitation is described as Eq. (3). The threshold for nutrient limitation in the model is calculated as Eqs. (4) and (5). Value of 1 indicates no limitation. During winter months, when the upper mixed layer is deep, the majority of the phytoplankton in the water column are light limited (< 0.8, Fig. 7A). During this period, nutrient limitation is low (> 0.8, Fig. 7B). As solar illumination increases in spring, the mixed layer depth shallows and light limitation is decreased; however the entrainment of nutrients to surface waters is decreased and nitrate limitation begins to increase as the phytoplankton grow rapidly. In the euphotic zone, where there is sufficient light for photosynthesis, the reduction of CO_2 to organic carbon fuels the rate of cell doubling and population growth. Thus, the availability light drives the flux of carbon, and other elements, into cells and thereby determines the rate at which nutrients are utilized by photoautotroph for growth (Dubinsky and Schofield, 2010).

To test the role of mixing in regulating phytoplankton bloom dynamics we conducted a series of model simulations where we compared the models driven by measured wind (as above) to hypothetical simulations where no wind was applied to the ocean. Comparisons of the simulations for both Zone 1 and Zone 2 are shown in Fig. 8. In Zone 1, the "no wind" condition resulted in fall blooms later in the season, which reflects the importance of wind-induced mixing combined with seasonal cooling to drive the convective overturn on the MAB. The "no wind" condition does not show convective overturn and replenishment of nutrients to the surface waters until several weeks later in the season (Fig. 9D). The mid-winter depression in the winter bloom is not present in the "no wind" simulation. The magnitude and timing of the winter bloom is strongly tied to storms, which induce mixing during the dim winter months leading to increased light limitation of the phytoplankton (Xu et al., 2011); therefore the "no wind" condition diminishes mixing and light limitation and allows for larger winter blooms. The decline in the winter light limitation is also visible in the "no wind" plot (Fig. 10A, black line). Finally, as the spring transition begins and the water column begins to stratify due to increased radiant heating, the phytoplankton in the "no wind" experiment showed a more rapid biomass decrease reflecting an earlier onset of nutrient limitation (Fig. 10A). For Zone 2, the "no wind" condition resulted in an earlier spring bloom (Fig. 8B) reflecting the earlier onset of
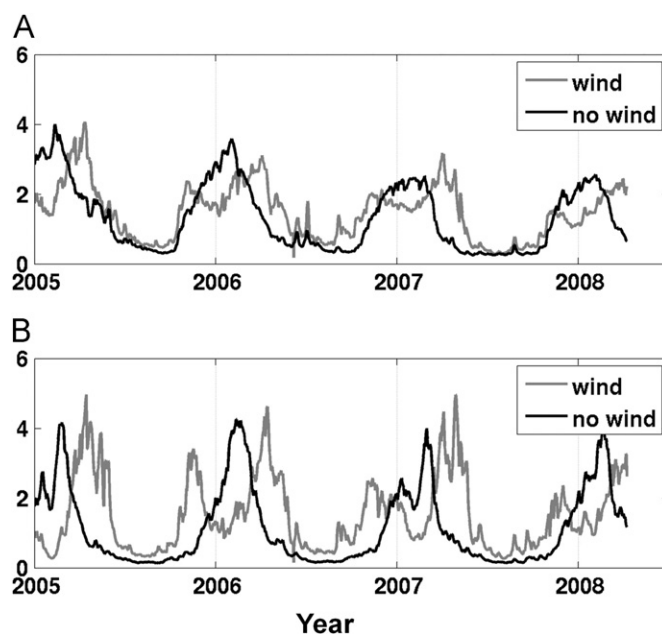

Fig. 8. Simulated time series of spatial mean surface chlorophyll concentration in Zone 1(A) and Zone 2(B). Black line represents the result under normal wind conditions; gray line represents the "no wind" forcing result.

stratification of the offshore waters. This is consistent with satellite analyses that suggested pre-spring storms strongly influenced the timing and magnitude of the spring bloom in the MAB (Xu et al., 2011). The other major differences in Zone 2, is that the spring phytoplankton activities were higher under the normal windy conditions (Fig. 8B), which alleviated the early onset of nutrient limitation as the MLD became shallower (Fig. 10B). Finally the fall bloom observed in Zone 2 was not present (Fig. 8B), as the convective overturn on the MAB was delayed and cells were nutrient limited (Fig. 10B).

3.3. Light, upper mixed layer depth, and chlorophyll

There is an inverse relationship between the MLD and the average light levels within the MLD (Fig. 11). Deeper mixed layers are associated with lower irradiance ($r = -0.84$, $p < 0.001$; $r = 0.72$, $p < 0.001$ for Zone 1 and Zone 2 respectively). This relationship
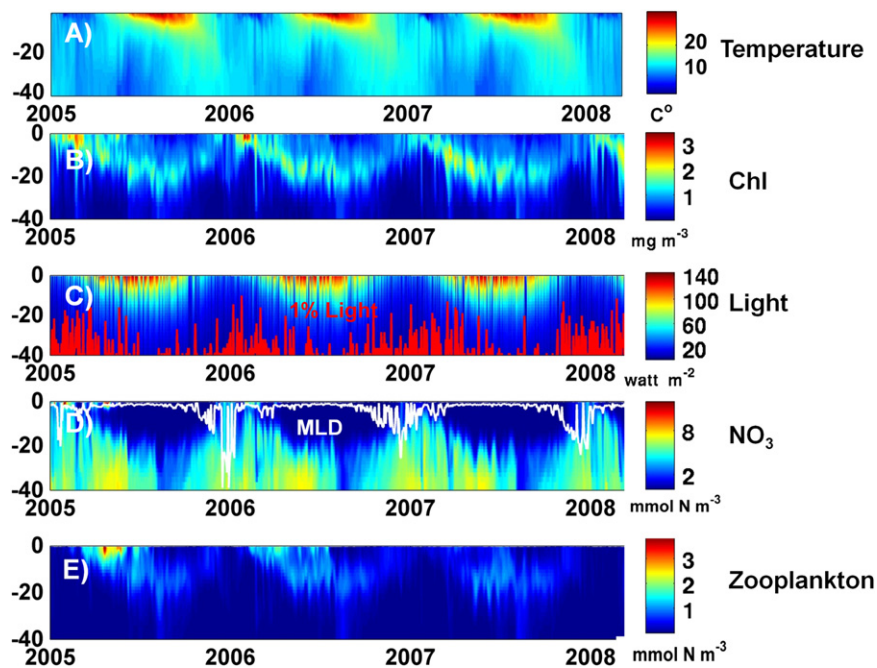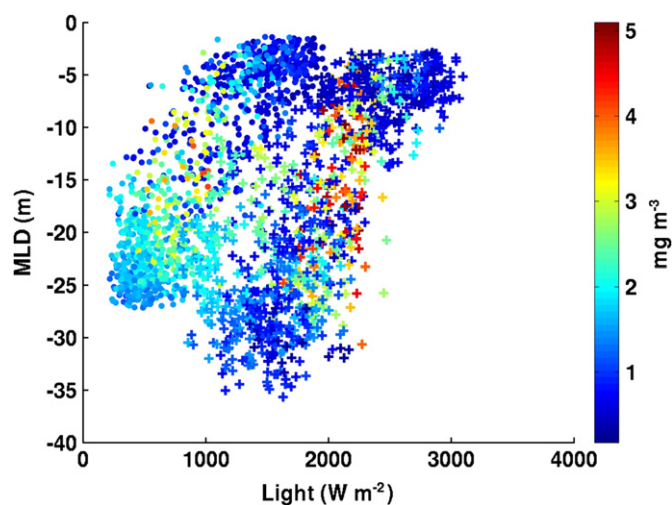
Fig. 9. Without wind forcing, the simulated vertical distribution of temperature (A) chlorophyll concentration (B), light (C), NO_3 (D) and zooplankton (E) in a dot located in Zone 1(dot shown in Fig. 1). The 1% light level depth is plotted with light (in C, red line) and the MLD is plotted with NO_3 (in (D), white line). (For interpretation of the references to color in this figure legend, the reader is referred to the web version of this article.)
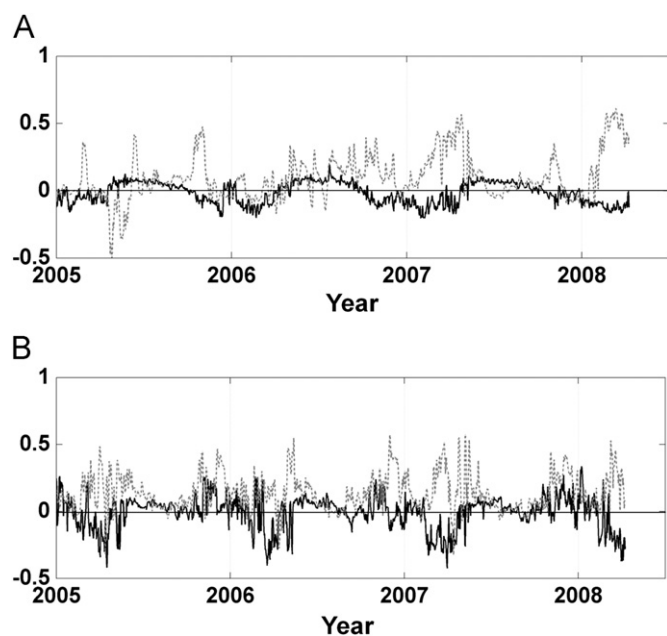
Fig. 10. Difference in light (black line) and nutrient (gray dashed line) limitation function between normal wind and no wind forcing condition in (A) Zone 1 and (B) Zone 2.

Fig. 11. Scatter plot of modeled mean light value in the mixed layer with MLD. The color represents the chlorophyll concentration in Zone 1 (dots) and Zone 2 (plus sign).

varies between Zone 1 and Zone 2, with offshore waters having a higher mean irradiance in the MLD. This reflects that the waters on the continental shelf are more turbid due to the enhanced attenuation of light by chlorophyll, colored dissolved organic matter and non-algal particles found in the shelf waters of the MAB (Schofield et al., 2004). While peak phytoplankton biomass ($> 4 \text{ mg m}^{-3}$) is found over a 5-fold range of MLDs, there is a narrow range (50%) of mean irradiances associated with peak phytoplankton concentrations (Fig. 8). Peak chlorophyll values in Zone 1 were associated with lower mean light intensities compared to Zone 2. In order to parameterize both the MLD and light critical threshold of light to

induce phytoplankton blooms we calculated mixing-light value (I') as the ratio of integral of light (I) in the euphotic zone (Z_{eu}) divided by the MLD (Z_{mld}) as

$$I' = \int_{-Z_{eu}}^{0} I(z)dz/Z_{mld} \qquad (6)$$

The I' term incorporates both the incident light and the mixing environment through the depth of the MLD. The MLD also contains information on the probability of nutrient availability. We assessed if there is a critical I' value associated with both the observed and simulated chlorophyll maximum (I'_{chlmax}). The I' values derived from the model were integrated into 20 W m^{-2} bins for Zone 1 and Zone 2 (Fig. 12). There is an increase in chlorophyll with increasing I' up until 60 and 160 W m^{-2} (I'_{chlmax}) for Zones 1 and Zone 2 respectively. Under these conditions,
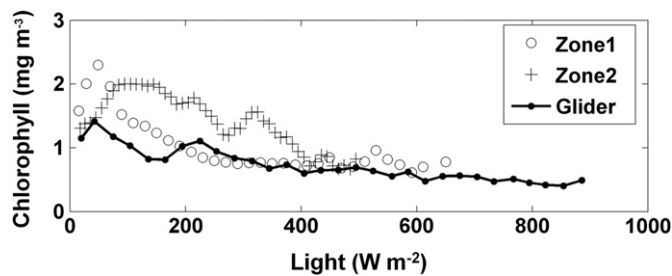
Fig. 12. Simulated mixed depth mean chlorophyll concentration and I' in every 20 W m^{-2}. I' value bins in Zone 1 (gray circle line) and Zone 2 (gray plus line), chlorophyll and I' based on glider observation are shown in black line with dots.

deeply mixed layers limited phytoplankton growth as overall light levels were low. For the waters of Zone 1 with shallow water depths, the mixed layer only need to decrease slightly to ensure that the majority of the water column is within the euphotic zone and phytoplankton have sufficient light to grow. In Zone 2, the deeper water depths require the MLD to decrease significantly in order to overcome light limitation. After this threshold has been reached, increasing I' is associated with declining chlorophyll. Here cells are maintained under high light but a shallow MLD does not allow for replenishment of the nutrients from depth. These chlorophyll and I' relationships were compared to chlorophyll data measured with Slocum gliders outfitted with fluorometers (Fig. 12, black line with dots). Despite that the glider data set is smaller and does not include many transects during the winter months, the relationship between I' and chlorophyll is similar showing an increase at low I' values to a value of 50 W m^{-2} and then decreasing values as I' increases. The glider chlorophyll values are lower than model estimates which is not surprising as the data set does not include many transects during the winter bloom. Calculations of I' for the "no wind" simulation show similar patterns except that it takes a high magnitude of I' to reach the peak chlorophyll values for Zone 2 (Fig. 15 plus line).

Is I'_{chlmax} predictable? Spatial maps of I'_{chlmax} associated with the chlorophyll maximum for the MAB are shown in Fig. 13. Generally, I'_{chlmax} is low and relatively constant on the continental shelf and increases in magnitude out over the continental slope and deep sea. The one shallow water exception was associated with the Hudson River plume, which is extremely turbid and mixing rates in the buoyant plume water must be high enough to overcome chronic light limitation for phytoplankton bloom Schofield et al., submitted for publication. Excluding this river zone, the relationship between I'_{chlmax} and bottom depth were robust (Fig. 14). Bottom depth could explain 70% of the variability in I'_{chlmax} ($p < 0.001$).

4. Discussion

The late fall-winter bloom is the most recurrent and largest phytoplankton bloom in the MAB (Xu et al., 2011; Yoder et al., 2001). The fall-winter bloom is fueled by the replenishment of nutrients to the euphotic zone once the summer thermal stratification has been disrupted. This thermal stratification is dramatic (summer thermoclines on the MAB exhibit a temperature gradient of over 15 °C in only 5 m water depth, cf. Castelao et al., 2010) and this stratification deprives the surface phytoplankton of macro and micronutrients throughout the late spring, summer and early autumn. Observational studies have documented there is a great deal of inter-annual variability in the timing of the late fall-winter bloom (Yoder et al., 2001). The variability in the timing of the bloom has been related to the timing of destratification,
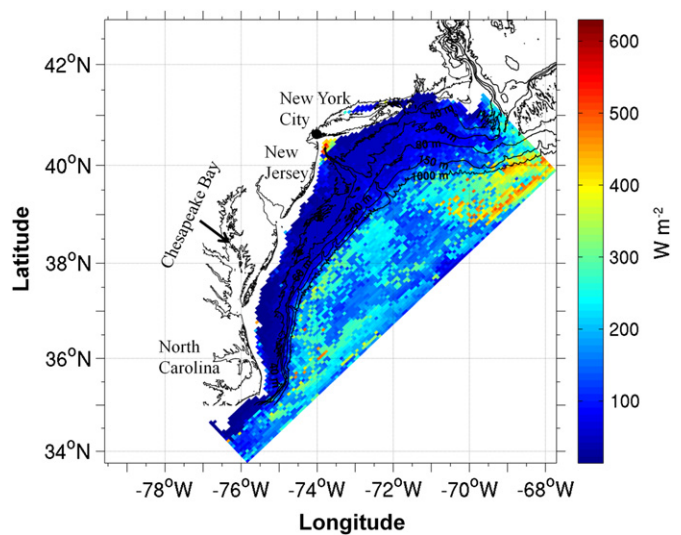

Fig. 13. The critical light value (I'_{chlmax}) in each grid of model domain.
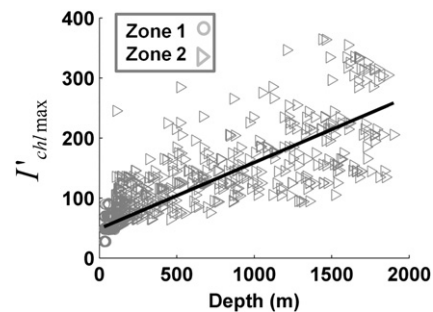

Fig. 14. Change of the critical light value with depth of all grids in Zone 1 (circle) and Zone 2 (triangle). Black line represents the linear regression of water depth and critical light value.
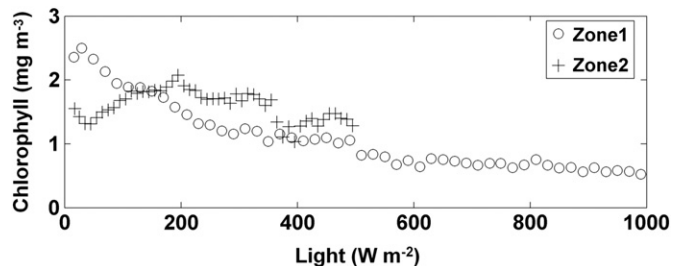

Fig. 15. Under no wind forcing, simulated mixed depth mean chlorophyll concentration and I' in every 20 W m^{-2} I' value bins in Zone 1 (red circle line) and Zone 2 (blue circle line), chlorophyll and I' based on glider observations are shown in black line with dots. (For interpretation of the references to color in this figure legend, the reader is referred to the web version of this article.)

which is driven by seasonal cooling of the surface waters and the passage of large storms that induce mixing (Beardsley et al., 1985; Glenn et al., 2008; Lentz et al., 2003). The magnitude of the fall-winter bloom is thought to be regulated by factors that stabilize the water column (Xu et al., 2011). In the MAB, these processes include the frequency of winter storms and the presence of low salinity buoyant plumes (Xu et al., 2011). While the observational data is compelling it has been insufficient to confirm the hypothesized forcing of the late fall-winter phytoplankton bloom.

To test the hypothesized physical forcing of the MAB phytoplankton we utilized the physical–biological ROMS model to conduct a series of simulations where we varied the physical forcing and analyzed the source and sinks of the phytoplankton.

The model which used realistic forcing was able to simulate the timing and spatial extent of the phytoplankton dynamics observed in SeaWiFS data. The model did a quantitatively good job of predicting the winter bloom; however the model had a more difficult time in reproducing the magnitude of the spring bloom. For the spring bloom region, there are large horizontal and vertical gradients in water properties and are associated with the shelf-break front, a feature susceptible to nonlinear instabilities and strong interactions with Gulf Stream warm-core rings (Gawarkiewicz et al., 2001, 2004). As a result, this region has complicated physical background that the mixing by wind cannot really be isolated. The discrepancy for the spring bloom likely reflected both by underestimated in chlorophyll by satellite-derived chlorophyll in this region (Fennel et al., 2006) and underestimated zooplankton grazing (Flagg et al., 1994). For the late fall-winter bloom, our numerical experiments explicitly demonstrated the role of wind-induced mixing in winter phytoplankton dynamics when all the other forcing factors were held constant. For the initiation of the late fall-winter bloom the no wind-induced mixing simulation demonstrated that wind was a secondary factor; therefore seasonal cooling and the corresponding convective overturn on the MAB is the dominant feature initiating the phytoplankton bloom. This is consistent with observations that tropical storms on the MAB can only induce water column turnover if the summer thermocline had been previously weakened by seasonal cooling (Glenn et al., 2008). After destratification, the frequency of high wind regulates the size of the phytoplankton bloom. Strong winds result in high mixing rates or less solar radiation because of cloudy weather, which results in the light limitation of the phytoplankton (Xu et al., 2011), which is confirmed by the model as an increased wind forcing resulted in smaller phytoplankton blooms.

Wind forcing also has a significant role on the timing and magnitude of the offshore spring bloom. Observational efforts have related the size and timing of the spring phytoplankton to the amount of wind-induced mixing present in the late winter (Xu et al., 2011). Wind-induced mixing in the late winter delays the thermal stratification of the MAB, which influences the spring bloom as cells require water column stabilization to overcome light limitation. During the no wind simulation, the spring bloom was dominated by a single event that occurred earlier in the season compared to normal wind conditions. This bloom was short lived as the cells rapidly consumed available nutrients. In contrast, the model simulation that used natural wind forcing resulted in a spring bloom that lasted longer throughout the season compared to the no wind condition as wind-induced mixing replenished the supply of nutrients and enhanced the overall amount of chlorophyll on the MAB. The SeaWiFS observed bloom in the shelf-break front region commenced in late March and lasted up to late April. In our simulated case with wind, the spring bloom in the shelf-break front region initiated in early March and lasted up to early April. It looks like that although the model simulated spring bloom start a little bit earlier under normal wind condition, it can better capture the both spring and fall bloom in this region compare with no wind forcing condition.

Is there a relatively predictable light condition that promotes a maximum chlorophyll concentration? Photosynthetic activity is confined to the euphotic zone, which is nominally defined as the depth where the light levels are 1% of the surface light intensity.

The depth of the euphotic zone is poor at predicting the initiation of phytoplankton blooms as any mixing to depth limits phytoplankton biomass accumulation in the upper mixed layer. This is due to the high respiratory costs to build cells (Falkowski and Raven, 2007). This discrepancy is accounted by Sverdrup's (1953) "critical depth" for bloom initiation (Obate et al., (1996);

Smetacek and Passow, 1990). This framework has been highly effective for the open ocean where the compensation depth for phytoplankton growth appears to be relatively constant (Siegel et al., 2002). In MAB, the light regime is tied closely to mixing regime as light is rapidly attenuated by high phytoplankton biomass and significant inputs from buoyant turbid plumes (Cahill et al., 2008; Castelao et al., 2008). As mixing determines not only the light but also the nutrient availability, there is need to parameterize the relative impacts of both. To parameterize the relative tradeoffs of mixing and light availability the ratio of Z_{mld} to Z_{eu} has been used to describe the regulating primary production (Huisman et al., 1999; Irigoien and Castel, 1997); however, this ratio only reflects the relationship between surface light condition and MLD. We suggest that it is more appropriate to use I' which is the ratio of integral of light in the euphotic zone and MLD to compare the balance between light limitation and nutrient limitation. When I' is low, phytoplankton are light-limited due to low surface irradiance and deep mixed layer. The variability shows a single peak in both the offshore and nearshore conditions. At high values of I', the mixed layer is shallow, coincident with the seasonal increase in solar illumination, which allowed the photosynthetic activity to consume the available nutrients. This in turn results in low biomass. We used the model to define this integral and then assess when it results in the maximum chlorophyll biomass (I'_{chlmax}). Model simulations suggest that on MAB, I'_{chlmax} varied by a factor of three and were spatially variable. The spatial variability was positively correlated with water depth, suggesting that this term can be parameterized.

Our results based on numerical simulation and glider observations confirm the SeaWiFS observation of seasonal phytoplankton bloom in the MAB. The modified light values are used to describe the balance between light and nutrients limitation and so as the influence the timing and magnitude of bloom. Sensitivity study of no wind forcing simulation proves that the mixing plays a significant role in regulating the nutrient and light field and thus influences the phytoplankton dynamics.

Acknowledgments

References

Beardsley, R.C., Chapman, D.C., Brink, K.H., Ramp, S.R., Schlitz, R., 1985. The Nantucket Shoals flux experiment (NSFE79). Part I: a basic description of the current and temperature variability. Journal of Physical Oceanography 15, 713–748.

Behrenfeld, M.J., Maranon, E., Siegel, D.A., Hooker, S.B., 2002. Photoacclimation and nutrient-based model of light-saturated photosynthesis for quantifying oceanic primary production. Marine Ecology Progress Series 228, 103–117, http://dx.doi.org/10.3354/meps228103.

Cahill, B., Schofield, O., Chant, R., Wilkin, J., Hunter, E., Glenn, S., Bissett, P., 2008. Dynamics of turbid buoyant plumes and the feedbacks on near-shore biogeochemistry and physics. Geophysical Research Letters 35, L10605, http://dx.doi.org/10.1029/2008GL033595.

Castelao, R., Schofield, O., Glenn, S., Chant, R., Kohut, J., 2008. Cross-shelf transport of freshwater on the New Jersey shelf. Journal of Geophysical Research 113, C07017, http://dx.doi.org/10.1029/2007JC004241.

Castelao, R., Glenn, S., Schofield, O., 2010. Temperature, salinity, and densty variability in the central Middle Atlantic Bight. Journal of Geophysical Research 115, C10005, http://dx.doi.org/10.1029/2009JC006082.

Dubinsky, Z., Schofield, O., 2010. From the light to the darkness: thriving at the light extremes in the oceans. Hydrobiologia 639, 153–171.

Dutkiewicz, S., Follows, M., Marshall, J., Gregg, W.W., 2001. Interannual variability of phytoplankton abundances in the North Atlantic. Deep Sea Research Part II:

Topical Studies in Oceanography 48, 2323–2344, http://dx.doi.org/10.1016/S0967-0645(00)00178-8.

Falkowski, P., Raven, J., 2007. Aquatic Photosynthesis, second ed.. Princeton University Press, Princeton.

Fairall, C.W., Bradley, E.F., Hare, J.E., Grachev, A.A., Edson, J.B., 2003. Bulk parameterization of air-sea fluxes: updates and verification for the coare algorithm. Journal of Climate 19 (4), 571–591.

Fasham, M.J.R., Ducklow, H.W., McKelvie, S.M., 1990. A nitrogen-based model of plankton dynamics in the oceanic mixed layer. Journal of Marine Research 48, 591–639.

Fennel, K., Wilkin, J., Levin, J., Moisan, J., O'Reilly, J., Haidvogel, D., 2006. Nitrogen cycling in the Middle Atlantic Bight: results from a three-dimensional model and implications for the North Atlantic nitrogen budget. Global Biogeochemical Cycles 20, GB3007, http://dx.doi.org/10.1029/2005GB002456.

Field, C.B., Behrenfeld, M.J., Randerson, J.T., Falkowski, P., 1998. Primary production of the biosphere: integrating terrestrial and oceanic components. Science 281 (5374), 237–240, http://dx.doi.org/10.1126/science.281.5374.237.

Flagg, C., Wirick, N., Smith, S. I., C.D., 1994. The interaction of phytoplankton, zooplankton and currents from 15 months of continuous data in the Mid-Atlantic Bight. Deep Sea Research Part II: Topical Studies in Oceanography 41, 411–435.

Gawarkiewicz, G., Bahr, F., Beardsley, R.C., Brink, K.H., 2001. Interaction of a slope eddy with the shelfbreak front in the Middle Atlantic Bight. Journal of Physical Oceanography 21, 2783–2796.

Gawarkiewicz, G., Brink, K.H., Bahr, F., Beardsley, R.C., Caruso, M., Lynch, J., Chiu, C.-S., 2004. A large-amplitude meander of the shelfbreak front in the Middle Atlantic Bight: observations from the Shelfbreak PRIMER experiment. Journal of geophysical research, 109, http://dx.doi.org/10.1029/2002JC001468.

Gentleman, W., Leising, A., Frost, B., Strom, S., Murray, J., 2003. Functional responses for zooplankton feeding on multiple resources: a review of assumption and biological dynamics. Deep Sea Research Part II: Topical Studies in Oceanography 50, 2847–2876.

Glenn, S.M., Jones, C., Twardowski, M., Bowers, L., Kerfoot, L., Webb, D., Schofield, O., 2008. Glider observations of sediment resuspension in a Middle Atlantic Bight fall transition storm. Limnology and Oceanography 53, 2180–2196.

Haidvogel, D.B., Beckmann, A., 1999. Numerical Ocean Circulation Modeling, Series on Environmental Science and Management, vol. 2. Imperial College Press, London 318 pp.

Hofmann, E.E., Cahill, B., Fennel, K., Friedrichs, M.A.M., Hyde, K., Lee, C., Mannino, A., Najjar, R.G., O'Reilly, J.E., Wilkin, J., Xue, J., 2011. Modeling the dynamics of continental shelf carbon. Annual Review of Marine Science 3, 93–122.

Howarth, et al., 1996. Regional nitrogen budgets and riverine N & P fluxes for the drainages to the North Atlantic Ocean: natural and human influences. Biogeochemistry 35, 181–226.

Huisman, J., Jonker, R.R., Zonneveld, C., Weissing, F.J., 1999a. Competition for light between phytoplankton species: experimental tests of mechanistic theory. Ecology 80, 211–222.

Irigoien, X., Castel, J., 1997. Light limitation and distribution of chlorophyll pigments in a highly turbid estuary: the Gironde (SW France). Estuarine, Coastal and Shelf Science 44, 507–517.

Lentz, S., Shearman, K., Anderson, S., Plueddemann, A., Edson, J., 2003. Evolution of stratification over the New England shelf during the coastal mixing and optics study, August 1996–June 1997. Journal of Geophysical Research 108 (C1), 3008, http://dx.doi.org/10.1029/2001JC001121.

Longhurst, A.R., 1998. Ecological Geography of the Sea. Academic Press, San Diego 398 pp.

Martin, H.J., 1965. Phytoplankton–zooplankton relationships in Narragansett Bay. Limnology and Oceanography 10, 185–191.

Obate, A., Ishizake, J., Endoh, M., 1996. Global verification of critical depth theory for phytoplankton bloom with climatological in situ temperature and satellite ocean color data. Journal of Geophysical Research 101, 20657–20667.

O'Reilly, J., Busch, D.A., 1984. Phytoplankton primary production on the north–west Atlantic Shelf. Rapports et Proces-Verbaux des Reunions Conseil International pour l'Exploration de la Mer. 183, pp. 255–268.

O'Reilly, J., Evans-Zetlin, E.C., Busch, D.A., 1987. Primary production. 220–233. In: Backus, R.H., Bourne, D.W. (Eds.), Georges Bank. MIT Press, Cambridge, MA.

O'Reilly, J., Zetlin, C., 1998. Seasonal, horizontal, and vertical distribution of phytoplankton chlorophyll a in the northeast US continental shelf ecosystem. NOAA Technical Report NMFS 139, US Department of Commerce.

Ryan, J.P., Yoder, J.A., Cornillon, P.C., 1999. Enhanced Chlorophyll at the Shelfbreak of the Mid-Atlantic Bight and Georges Bank during the Spring Transition. Limnology and Oceanography 44, 1–11.

Ryther, J.H., Dunstan, W.M., 1971. Nitrogen, phosphorus, and eutrophication in the coastal marine environment. Science 171, 1008–1112.

Schofield, O., Bergmann, T., Oliver, M., Irwin, A., Kirkpatrick, G., Bissett, W.P., Orrico, C., Moline, M.A., 2004. Inverting inherent optical signatures in the nearshore coastal waters at the long term ecosystem observatory. Journal of Geophysical Research 109, C12S04, http://dx.doi.org/10.1029/2003JC002071.

Schofield, O., et al., 2007. Slocum gliders: robust and ready. Journal of Field Robotics 24, 1–14, http://dx.doi.org/10.1009/rob.20200.

Schofield, O., et al., 2010. Automated sensor networks to advance ocean science. Transaction of the American Geophysical Union 91 (39), 345–346, http://dx.doi.org/10.1029/2010EO390001.

Schofield, O., Chant, R., Hunter, E., Moline, M.A., Reinfelder, J., Glenn, S.M., Frazer, T., Optical transformations in a turbid buoyant plume. Continental Shelf Research, submitted for publication.

Sharp, J.H., Church, T.M., 1981. Biochemical modeling in coastal waters of the Middle Atlantic States. Limnology and Oceanography 26 (5), 843–854.

Siegel, D.A., Doney, S.C., Yoder, J.A., 2002. The North Atlantic spring phytoplankton bloom and Sverdrup's critical depth hypothesis. Science 296, 730–733.

Smetacek, V., Passow, U., 1990. Spring bloom initiation and Sverdrup's critical depth model. Limnology and Oceanography 35 (1), 228–234.

Sverdrup, H.U., 1953. On conditions for the vernal blooming of phytoplankton. Journal du Conseil International pour l'Exploration de la Mer 18, 287–295.

Tilman, D., 1982. Resource competition and community structure. Princeton University Press, Princeton, NJ, USA.

Turner, J.T., Tester, P.A., 1997. Toxic marine phytoplankton, zooplankton grazers, and pelagic food webs. Limnology and Oceanography 42, 1203–1214.

Wilkin, J.L., Arango, H.G., Haidvogel, D.B., Lichtenwalner, C.S., Glenn, S.M., Hedstrom, K.S., 2005. A regional ocean modeling system for the Long-term ecosystem observatory. Journal of Geophysical Research 110, C06S91, http://dx.doi.org/10.1029/2003JC002218.

Xu, Y., Chant, R., Gong, D., Castelao, R., Glenn, S., Schofield, O., 2011. Seasonal variability of chlorophyll a in the Mid-Atlantic Bight. Continental Shelf Research 31, 1640.

Yoder, J.A., O'Reilly, J.E., Barnard, A.H., Moore, T.S., Ruhsam, C.M., 2001. Variability in coastal zone color scanner (CZCS) Chlorophyll imagery of ocean margin waters off the US East Coast. Continental Shelf Research 21, 1191–1218.